



Cite this: *Chem. Commun.*, 2015, 51, 14326

Received 16th July 2015,  
Accepted 5th August 2015

DOI: 10.1039/c5cc05931c

www.rsc.org/chemcomm

## Characterization of a heterobimetallic nonheme Fe(III)–O–Cr(III) species formed by O<sub>2</sub> activation†

Ang Zhou, Scott T. Kleespies, Katherine M. Van Heuvelen‡ and Lawrence Que Jr.\*

**We report the generation and spectroscopic characterization of a heterobimetallic [(TMC)Fe<sup>III</sup>–O–Cr<sup>III</sup>(OTf)<sub>4</sub>] species (**1**) by bubbling O<sub>2</sub> into a mixture of Fe(TMC)(OTf)<sub>2</sub> and Cr(OTf)<sub>2</sub> in NCCH<sub>3</sub>. Complex **1** also formed quantitatively by adding Cr(OTf)<sub>2</sub> to [Fe<sup>IV</sup>(O)(TMC)(NCCH<sub>3</sub>)]<sup>2+</sup>. The proposed O<sub>2</sub> activation mechanism involves the trapping of a Cr–O<sub>2</sub> adduct by Fe(TMC)(OTf)<sub>2</sub>.**

Oxygen activation is generally carried out by metalloenzymes with mononuclear or homodinuclear iron or copper active sites.<sup>1–3</sup> However there are two notable exceptions to this generalization, namely the heme/copper center of cytochrome oxidase essential for mammalian respiration<sup>1,4,5</sup> and the nonheme Fe–O–Mn center of Class 1c ribonucleotide reductases found in pathogenic bacteria.<sup>6,7</sup> There has been significant progress in obtaining synthetic models for the heme/copper center of cytochrome oxidase,<sup>8–10</sup> but less effort has been devoted to the synthesis of nonheme (μ-oxo)heterobimetallic complexes. In 1992 Wiegardt described a series of carboxylate-bridged (TACN)Fe<sup>III</sup>–O–M(Me<sub>3</sub>TACN) (M = Cr<sup>III</sup> or Mn<sup>III</sup>, TACN = 1,4,7-triazacyclononane, Me<sub>3</sub>TACN = 1,4,7-trimethyl-1,4,7-triazacyclononane) complexes obtained by hydrolysis between FeCl<sub>3</sub>(TACN) and MCl<sub>3</sub>(Me<sub>3</sub>TACN) precursors.<sup>11</sup> More recently, Fukuzumi and Nam reported the crystal structure of a novel Fe<sup>III</sup>–O–Sc<sup>III</sup> complex, which was obtained from the reaction of [Fe<sup>IV</sup>(O)(TMC)(NCCH<sub>3</sub>)]<sup>2+</sup> (TMC = 1,4,8,11-tetramethylcyclam) with Sc(OTf)<sub>3</sub>.<sup>12</sup> However, no synthetic nonheme Fe–O–M complex (where M is a non-iron metal) has thus far been generated by O<sub>2</sub> activation. Here we report the characterization of [(TMC)Fe<sup>III</sup>–O–Cr<sup>III</sup>(OTf)<sub>4</sub>] (**1**) formed by oxygenating a mixture of Fe(TMC)(OTf)<sub>2</sub> and Cr(OTf)<sub>2</sub> in CH<sub>3</sub>CN at –40 °C or reacting [Fe<sup>IV</sup>(O)(TMC)(NCCH<sub>3</sub>)]<sup>2+</sup> with 1 eq. of Cr(OTf)<sub>2</sub>.

Department of Chemistry and Center for Metals in Biocatalysis,  
University of Minnesota, 207 Pleasant St. SE, Minneapolis, Minnesota 55455, USA.  
E-mail: larryque@umn.edu

† Electronic supplementary information (ESI) available: Instrumental methods, synthetic procedures, and structural characterization. See DOI: 10.1039/c5cc05931c

‡ Current address: Department of Chemistry, Harvey Mudd College, Claremont, CA 91711, USA.

Bubbling O<sub>2</sub> into a solution of 1 mM Fe(TMC)(OTf)<sub>2</sub> and 1 mM Cr(OTf)<sub>2</sub> in CH<sub>3</sub>CN at –40 °C rapidly elicited a UV-vis spectrum with bands at 358, 398, 447 and 558 nm (Fig. 1), suggesting the formation of a new species designated as **1**. This spectral pattern was not observed in the absence of either Fe(TMC)(OTf)<sub>2</sub> or Cr(OTf)<sub>2</sub> from the reaction mixture; Fe(TMC)(OTf)<sub>2</sub> simply did not react with O<sub>2</sub>, but the reaction of Cr(OTf)<sub>2</sub> with O<sub>2</sub> gave rise to features at 358 and 445 nm (Fig. 1), distinct from those of **1**. Species **1** had a half-life of 10 h at –40 °C and rapidly decayed upon warming to RT. Taken together, these observations implicate both Fe and Cr in the formation of **1**.

ESI-MS analysis of the solution of **1** at –40 °C revealed dominant peaks at *m/z* 461.2 (positive mode) and 514.8 (negative mode) (Fig. S1, ESI†), which were not observed in oxygenated solutions lacking either Fe(TMC)(OTf)<sub>2</sub> or Cr(OTf)<sub>2</sub>. The ions observed have masses and isotope distribution patterns that correspond to [Fe(TMC)(OTf)]<sup>+</sup> and [CrO(OTf)<sub>3</sub>]<sup>–</sup>, respectively. Furthermore, the [CrO(OTf)<sub>3</sub>]<sup>–</sup> peak was upshifted by 2 units when <sup>18</sup>O<sub>2</sub> was used, showing the incorporation of an oxygen atom from O<sub>2</sub> (Fig. S2, ESI†). Based on these results, we tentatively assign **1** as a heterobimetallic [(TMC)Fe<sup>III</sup>–O–Cr<sup>III</sup>(OTf)<sub>4</sub>] complex, which undergoes homolysis of the Fe–O bond to give rise to the observed mass spectral features.

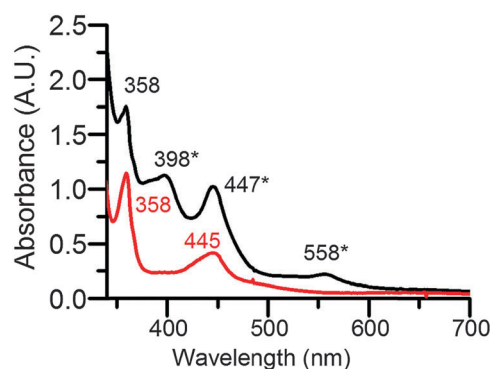


Fig. 1 UV-vis spectra observed in CH<sub>3</sub>CN at –40 °C upon O<sub>2</sub> exposure of 1 mM Cr(OTf)<sub>2</sub> (red) and a mixture of 1 mM Fe(TMC)(OTf)<sub>2</sub> and 1 mM Cr(OTf)<sub>2</sub> (black). Bands with asterisks are associated with **1**.



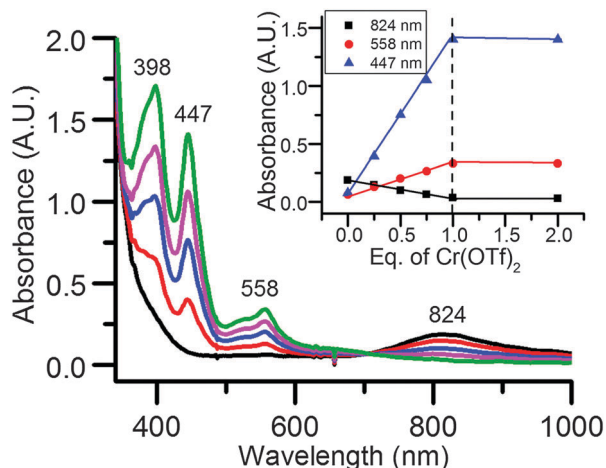


Fig. 2 UV-vis spectral titration of 0.45 mM  $[\text{Fe}^{\text{IV}}(\text{O})(\text{TMC})(\text{NCCH}_3)]^{2+}$  in  $\text{CH}_3\text{CN}$  at  $-40^\circ\text{C}$  with  $\text{Cr}(\text{OTf})_2$ . Black, 0 eq.; red, 0.25 eq.; blue: 0.5 eq.; magenta, 0.75 eq.; green, 1 eq. Inset: Titration plot. Inset: Formation of **1** vs. eq.  $\text{Cr}(\text{OTf})_2$  added into 0.45 mM  $[\text{Fe}^{\text{IV}}(\text{O})(\text{TMC})(\text{NCCH}_3)]^{2+}$  in  $\text{CH}_3\text{CN}$  at  $-40^\circ\text{C}$ .

To test this hypothesis, we investigated the reaction of  $[\text{Fe}^{\text{IV}}(\text{O})(\text{TMC})(\text{NCCH}_3)]^{2+}$  with  $\text{Cr}(\text{OTf})_2$  in  $\text{CH}_3\text{CN}$  at  $-40^\circ\text{C}$  as a more direct means of synthesizing putative species **1**. As shown in Fig. 2, the addition of  $\text{Cr}(\text{OTf})_2$  to  $[\text{Fe}^{\text{IV}}(\text{O})(\text{TMC})(\text{NCCH}_3)]^{2+}$  in  $\text{CH}_3\text{CN}$  solution caused the instantaneous disappearance of its characteristic 824 nm peak concomitant with the growth of bands at 398, 447, and 558 nm that are assigned to **1**. Titration experiments (Fig. 2, inset) revealed that the transformation was complete upon addition of 1 eq.  $\text{Cr}(\text{OTf})_2$ , strongly suggesting a 1:1 Fe:Cr stoichiometry for **1**. This solution also gave rise to ESI-MS spectra with the same dominant peaks as the complex generated by  $\text{O}_2$  activation. A control experiment between  $\text{Cr}(\text{OTf})_2$  and  $\text{PhIO}$  did not elicit the same peaks as found in **1** (Fig. S3, ESI<sup>†</sup>), suggesting that  $[\text{Fe}^{\text{IV}}(\text{O})(\text{TMC})(\text{NCCH}_3)]^{2+}$  acts more than just an oxygen atom donor to  $\text{Cr}(\text{OTf})_2$ . These results demonstrate that **1** can be generated by either  $\text{O}_2$  activation or inner-sphere electron transfer.

In order to obtain structural insight, Fe K-edge X-ray absorption spectroscopy studies were carried out on **1**. As shown in Fig. S4 (ESI<sup>†</sup>), the Fe K-edge of **1** was found at 7124.0 eV, which is comparable to those of known  $\text{Fe}^{\text{III}}(\text{TMC})$  and related complexes.<sup>14</sup> Species **1** also exhibits a pre-edge feature that is associated with 1s-to-3d transitions with an area of 11 units. The Fourier-transformed EXAFS region revealed two prominent features at  $R + \Delta \sim 1.8 \text{ \AA}$  and  $3.2 \text{ \AA}$  (Fig. 3, left). The best fit of the data (fit #8 in Table S1, ESI<sup>†</sup>) consisted of 1 O/N scatterer at 1.81  $\text{Å}$ , 5 O/N scatterers at 2.17  $\text{Å}$ , 4 C scatterers at 2.91  $\text{Å}$  and a Cr scatterer at a distance of 3.65  $\text{Å}$ . The 2.17  $\text{Å}$  and 2.92  $\text{Å}$  scatterers arise from the supporting TMC ligand, while the 1.81  $\text{Å}$  scatterer has an Fe–O distance typically found for oxo bridges in  $\text{Fe}^{\text{III}}\text{--O--M}^{\text{III}}$  complexes.<sup>15</sup> The 3.2  $\text{Å}$  feature corresponds to a Cr scatterer at 3.65  $\text{Å}$ ; its intensity derives from multiple scattering pathways due to a linear Fe–O–Cr core. Indeed, the Fe···Cr distance is typical of the metal–metal distances found for linear  $\text{Fe}^{\text{III}}\text{--O--M}^{\text{III}}$  complexes<sup>12,16,17</sup> and exemplified by  $[(\text{py})(\text{TPP})\text{Cr}^{\text{III}}\text{--O--Fe}^{\text{III}}(\text{TMP})]$  ( $r(\text{Fe} \cdots \text{Cr}) = 3.60 \text{ \AA}$ ; py = pyridine; TPP = tetraphenylporphyrin

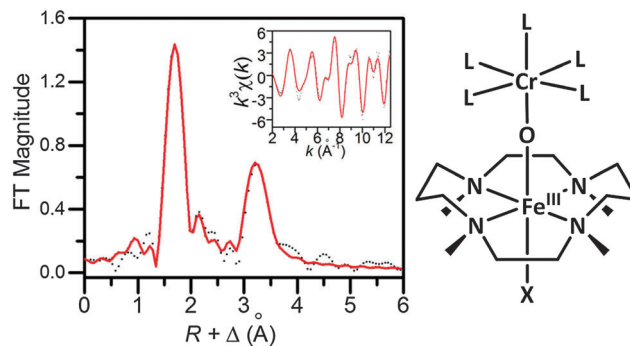


Fig. 3 Left: Fourier-transformed Fe K-edge EXAFS data for **1** (dotted black line) and corresponding best fit (solid red line, fit #8 in Table S1, ESI<sup>†</sup>). Inset shows unfiltered  $k$ -space data and its fit. Right: Proposed structure for **1** ( $L = \text{CH}_3\text{CN}$  or  $\text{OTf}$ ;  $X = \text{CH}_3\text{CN}$ ,  $\text{NCO}$  or  $\text{NCS}$ ).

dianion; TMP = tetramesitylporphyrin dianion).<sup>18</sup> We thus propose that **1** has the structure shown in Fig. 3 right.

The proposed structure for **1** resembles that found in the crystal structures of the recently described  $[(\text{TMC})\text{Fe}^{\text{III}}\text{--O--Sc}^{\text{III}}(\text{OTf})_4(\text{L})]$  complex (**2**,  $L = \text{H}_2\text{O}$  or  $\text{NCCH}_3$ ).<sup>12</sup> However, they differ in several respects. Although the Fe···M distances are essentially identical for **1** and **2**, the respective Fe–O and M–O distances are distinct. The Fe–O distance of 1.81  $\text{Å}$  for **1** is 0.07  $\text{Å}$  longer than that found for **2**, while the Cr–O distance of 1.84  $\text{Å}$  (deduced from the difference between the Fe···Cr and the Fe–O distances from the EXAFS analysis, assuming  $\angle \text{Fe--O--Cr} \sim 180^\circ$ ) is 0.07  $\text{Å}$  shorter than the Sc–O distance of 1.91  $\text{Å}$  observed for **2** in its crystal structures. The distinct M–O distances in **1** and **2** presumably reflect the difference between the more covalent Cr–O bond and the more ionic Sc–O bond, which also affect the corresponding Fe–O bond. Another feature distinguishing **1** from **2** is the intensity of the XAS pre-edge feature. Complex **1** exhibits a pre-edge area of 11 units, typical of a six-coordinate iron(III) center,<sup>19,20</sup> while **2** ( $L = \text{NCCH}_3$ ) has a much larger pre-edge area of 32 units,<sup>12</sup> reflecting the square pyramidal geometry of its iron(III) center. Lastly, the four methyl groups of the TMC ligand are shown in Fig. 3 right as being oriented *anti* with respect to the oxo bridge, opposite to the orientation found crystallographically for the methyl groups in **2**.<sup>12</sup> Although we do not have direct proof, our main argument to favor the *anti* orientation over the *syn* one is the observed immediate formation of **1** upon  $\text{Cr}(\text{OTf})_2$  addition to a solution of  $[\text{Fe}^{\text{IV}}(\text{O})(\text{TMC})(\text{NCCH}_3)]^{2+}$ . As the TMC methyl groups are oriented *anti* to the oxo moiety in the precursor,<sup>13</sup> it seems unlikely that a change in their relative orientations could occur at  $-40^\circ\text{C}$  within this very short time scale.

The likelihood of a sixth ligand for the iron(III) center in **1** is supported by the change in the spectral features of **1** upon addition of  $\text{NCS}^-$  or  $\text{NCO}^-$ . As shown in Fig. 4, there are small shifts of the three bands, as well as increases in intensity. Titration experiments showed that only 1 eq. of  $\text{NCS}^-$  or  $\text{NCO}^-$  was needed to transform **1** fully into **1-NCS** or **1-NCO** (Fig. S5 and S6, ESI<sup>†</sup>). ESI-MS analysis of **1-NCS** and **1-NCO** revealed respective positive mode peaks at  $m/z$  370 and 354, corresponding to  $[\text{Fe}(\text{TMC})(\text{NCS})]^+$  and  $[\text{Fe}(\text{TMC})(\text{NCO})]^+$  fragment ions (Fig. S7 and S8, ESI<sup>†</sup>), suggesting the occupation of the axial position *trans* to the



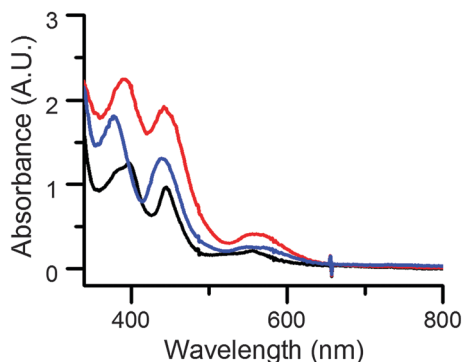


Fig. 4 UV-vis spectra of 0.3 mM **1** (black), **1-NCO** (blue), **1-NCS** (red) in CH<sub>3</sub>CN at -40 °C.  $\lambda_{\max}$  ( $\epsilon_M$ ) for **1**: 398 (3800), 447 (3000), and 558 (700).  $\lambda_{\max}$  ( $\epsilon_M$ ) for **1-NCO**: 380 (6000), 438 (4200), and 560 (850).  $\lambda_{\max}$  ( $\epsilon_M$ ) for **1-NCS**: 390 (7500), 442 (6300), and 560 (1400).

oxo bridge by these anions. Furthermore, **1-NCS** exhibits an Fe K-edge energy of 7124.3 eV, comparable to the 7124.0 eV value found for **1**. **1-NCS** also exhibits a pre-edge feature with an area of 9 units (Fig. S9, ESI<sup>†</sup>), which is close to the 11 units found for **1** but much smaller than the 32 units associated with **2**, showing that a six-coordinate iron(III) center in **1-NCS** is maintained. EXAFS analysis of **1-NCS** shows the presence of a linear Fe–O–Cr core like that in **1**, but with a 1.85 Å Fe–O bond and an Fe...Cr distance of 3.67 Å (Table S2 and Fig. S10, ESI<sup>†</sup>). The observed lengthening of the Fe–O bond can be rationalized by the axial NCS<sup>-</sup> binding to the iron(III) center. Based on all the information above, **1** is proposed to be a heterobimetallic  $\mu$ -oxo species with an Fe–O–Cr core, and the Fe atom has a 6-coordinate environment with the axial position available for ligand substitution (Fig. 3, right).

Complex **1** was further studied by EPR and resonance Raman spectroscopy. It is EPR-silent, which is as expected due to antiferromagnetic coupling mediated by the oxo bridge between the Fe(III) and the Cr(III) centers, as seen for two other Fe(III)–O–Cr(III) complexes.<sup>11,18</sup> Excitation of **1** with a 568.2 nm laser elicits a resonance-enhanced vibration at 773 cm<sup>-1</sup> (Fig. 5), which falls within the 700–900 cm<sup>-1</sup> range found for the  $\nu_{\text{as}}(\text{Fe–O–Fe})$  modes of oxo-bridged diiron(III) complexes.<sup>21</sup> This assignment is corroborated by the observed downshift of

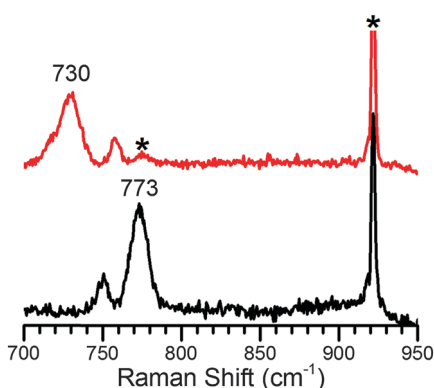
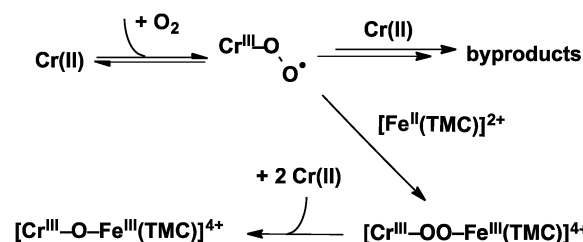


Fig. 5 Resonance Raman spectra of **1** in CH<sub>3</sub>CN ( $\lambda_{\text{ex}} = 568.2$  nm, 20 mW, 77 K). Black, <sup>16</sup>O; red, <sup>18</sup>O. Asterisks denote solvent peaks.

this vibration to 730 cm<sup>-1</sup> upon <sup>18</sup>O-substitution into the oxo bridge. Although a 35 cm<sup>-1</sup> downshift for a diatomic Fe–O mode is predicted by Hooke's Law, the experimentally obtained <sup>18</sup>O shift is 43 cm<sup>-1</sup>. This larger than predicted shift has also been reported for corresponding vibrations of several oxo-bridged diiron(III) complexes.<sup>21</sup> There is also a weaker feature found at 746 cm<sup>-1</sup> that exhibits an upshift of 7 cm<sup>-1</sup> upon <sup>18</sup>O-substitution; this is an unusual observation that we cannot explain. The 773 cm<sup>-1</sup> vibration is also weakly enhanced upon 514.5 nm excitation but not observed with 457.9 or 647.1 nm irradiation, suggesting that the 558 nm absorption band can be associated with a transition of the Fe–O–Cr moiety.

With the nature of **1** reasonably well characterized, we return to an analysis of the O<sub>2</sub> activation reaction results. Based on the molar extinction coefficients of **1** determined from the stoichiometric conversion of [Fe<sup>IV</sup>(O)(TMC)(NCCH<sub>3</sub>)<sub>2</sub>]<sup>2+</sup> to **1** by Cr(OTf)<sub>2</sub>, we conclude that **1** is produced in about 30% yield from the reaction of equimolar amounts of Fe(TMC)(OTf)<sub>2</sub> and Cr(OTf)<sub>2</sub> to O<sub>2</sub>. The yield of **1** was unchanged by increasing the Fe(TMC)(OTf)<sub>2</sub>/Cr(OTf)<sub>2</sub> ratio from 1 to 10 ([Cr(OTf)<sub>2</sub>] = 1 mM) (Fig. S11, ESI<sup>†</sup>), suggesting that Cr(OTf)<sub>2</sub> is the limiting reagent. In contrast, the yield of **1** increased to 95% when the concentration of Fe(TMC)(OTf)<sub>2</sub> was fixed at 1 mM and the Cr(OTf)<sub>2</sub> concentration was raised from 1 mM to 10 mM (Fig. S12, ESI<sup>†</sup>). Therefore, the % yield of **1** is dependent on the amount of Cr(OTf)<sub>2</sub>, but not on the amount of Fe(TMC)(OTf)<sub>2</sub>. These results can be rationalized by the O<sub>2</sub> activation pathway proposed in Scheme 1, in which the four electrons needed to reduce O<sub>2</sub> to the oxidation level of water are provided by 1 eq. Fe(TMC)(OTf)<sub>2</sub> and 3 eq. Cr(OTf)<sub>2</sub>, not unlike the four redox-active centers required for O<sub>2</sub> activation by cytochrome oxidase.<sup>4</sup> In the present case, we postulate that O<sub>2</sub> initially binds to the O<sub>2</sub>-sensitive Cr(OTf)<sub>2</sub> to form a transient adduct (analogous to that characterized by Nam in the reaction of [Cr<sup>II</sup>(TMC)Cl]<sup>+</sup> with O<sub>2</sub><sup>22</sup>) that is then trapped by Fe(TMC)(OTf)<sub>2</sub> to generate a yet unobserved Fe<sup>III</sup>–O–O–Cr<sup>III</sup> peroxo-bridged intermediate. This intermediate is then reduced by another 2 eq. Cr(OTf)<sub>2</sub> to form **1**. Thus the *ca.* 30% yield of **1** observed under limiting Cr conditions reflects the 1:3 stoichiometry of Fe(TMC)(OTf)<sub>2</sub>/Cr(OTf)<sub>2</sub> needed to make **1**. On the other hand, under limiting Fe conditions, enough Cr–O<sub>2</sub> adduct is formed to react with all the available Fe(TMC)(OTf)<sub>2</sub> to convert the latter almost quantitatively to **1**.

In conclusion, a heterobimetallic nonheme species **1** with an Fe–O–Cr core has been generated from both O<sub>2</sub> activation and



Scheme 1 Proposed mechanism for formation of **1** by O<sub>2</sub> activation.



inner-sphere electron transfer. The structure of **1** was deduced by a combination of UV-vis, resonance Raman, and X-ray absorption spectroscopic methods and ESI-MS. The O<sub>2</sub> activation mechanism for the formation of **1** is proposed to be analogous to that of cytochrome oxidase, where the initially formed O<sub>2</sub> adduct is reduced by the other three redox-active metal centers in the enzyme, demonstrating a general strategy for O<sub>2</sub> activation. Furthermore, **1** represents only the second example of a hetero-bimetallic M–O–Fe(TMC) complex, which can shed light on the effects of Lewis acidic metal centers on the redox properties of high-valent M = O species.<sup>23</sup> Such interactions are considered important for facilitating the oxidation of water by the CaMn<sub>4</sub>O<sub>5</sub> cluster of the oxygen evolving complex in photosynthesis.<sup>24–26</sup> Along these lines, Lloret-Fillol and coworkers have demonstrated the formation of a related Fe<sup>IV</sup>–O–Ce<sup>IV</sup> intermediate in the oxidation of water by a nonheme iron catalyst with Ce(NH<sub>4</sub>)<sub>3</sub>(NO<sub>3</sub>)<sub>6</sub> as oxidant.<sup>27</sup>

This work was supported by a grant from the US National Institutes of Health (GM-38767 to L.Q.) and a postdoctoral fellowship (GM-093479 to K.M.V.H.). XAS data were collected on Beamline X3B at the National Synchrotron Light Source, which is supported by the U.S. Department of Energy under Contract No. DE-AC02-98CH10886. Use of beamline X3B is made possible by the Center for Synchrotron Biosciences grant, P30-EB-00998, from the National Institute of Biomedical Imaging and Bioengineering. XAS data were also collected on Beamline 7-3 at the Stanford Synchrotron Radiation Lightsource, which is supported by the U.S. Department of Energy under Contract No. DE-AC02-76SF00515. Use of beamline 7-3 is supported by the DOE Office of Biological and Environmental Research, and by the National Institutes of Health, National Institute of General Medical Sciences (including P41GM103393).

## References

- I. Bertini, H. Gray, E. I. Stiefel and J. S. Valentine, *Biological Inorganic Chemistry: Structure and Reactivity*, University Science Books, 2007, pp. 319–442.
- L. Que Jr. and W. B. Tolman, *Nature*, 2008, **455**, 333–340.
- E. I. Solomon, D. E. Heppner, E. M. Johnston, J. W. Ginsbach, J. Cirera, M. Qayyum, M. T. Kieber-Emmons, C. H. Kjaergaard, R. G. Hadt and L. Tian, *Chem. Rev.*, 2014, **114**, 3659–3853.
- S. Ferguson-Miller and G. T. Babcock, *Chem. Rev.*, 1996, **96**, 2889–2908.
- T. Tsukihara, H. Aoyama, E. Yamashita, T. Tomizaki, H. Yamaguchi, K. Shinzawa-Itoh, R. Nakashima, R. Yaono and S. Yoshikawa, *Science*, 1996, **272**, 1136–1144.
- W. Jiang, D. Yun, L. Saleh, E. W. Barr, G. Xing, L. M. Hoffart, M.-A. Maslak, C. Krebs and J. M. Bollinger, *Science*, 2007, **316**, 1188–1191.
- W. Jiang, D. Yun, L. Saleh, J. M. Bollinger Jr. and C. Krebs, *Biochemistry*, 2008, **47**, 13736–13744.
- T. Chishiro, Y. Shimazaki, F. Tani, Y. Tachi, Y. Naruta, S. Karasawa, S. Hayami and Y. Maeda, *Angew. Chem., Int. Ed.*, 2003, **42**, 2788–2791.
- E. Kim, E. E. Chufan, K. Kamaraj and K. D. Karlin, *Chem. Rev.*, 2004, **104**, 1077–1134.
- E. E. Chufan, S. C. Puiu and K. D. Karlin, *Acc. Chem. Res.*, 2007, **40**, 563–572.
- R. Hotzelmann, K. Wieghardt, U. Floerke, H. J. Haupt, D. C. Weatherburn, J. Bonvoisin, G. Blondin and J. J. Gierd, *J. Am. Chem. Soc.*, 1992, **114**, 1681–1696.
- (a) S. Fukuzumi, Y. Morimoto, H. Kotani, P. Naumov, Y.-M. Lee and W. Nam, *Nat. Chem.*, 2010, **2**, 756–759; (b) M. Swart, *Chem. Commun.*, 2013, **49**, 6650–6652; (c) J. Prakash, G. T. Rohde, K. K. Meier, A. J. Jasniowski, K. M. Van Heuvelen, E. Münck and L. Que Jr., *J. Am. Chem. Soc.*, 2015, **137**, 3478–3481.
- J.-U. Rohde, J.-H. In, M. H. Lim, W. W. Brennessel, M. R. Bukowski, A. Stubna, E. Münck, W. Nam and L. Que, Jr., *Science*, 2003, **299**, 1037–1039.
- (a) F. Li, *PhD thesis*, University of Minnesota, 2011; (b) K. D. Koehntop, J.-U. Rohde, M. Costas and L. Que Jr., *Dalton Trans.*, 2004, 3191–3198; (c) X. Shan, J.-U. Rohde, K. D. Koehntop, Y. Zhou, M. R. Bukowski, M. Costas, K. Fujisawa and L. Que, Jr., *Inorg. Chem.*, 2007, **46**, 8410–8417.
- D. M. Kurtz Jr., *Chem. Rev.*, 1990, **90**, 585–606.
- S. C. Lee and R. Holm, *J. Am. Chem. Soc.*, 1993, **115**, 11789–11798.
- J. F. Berry, E. Bill, R. Garcia-Serres, F. Neese, T. Weyhermüller and K. Wieghardt, *Inorg. Chem.*, 2006, **45**, 2027–2037.
- D. J. Liston, B. J. Kennedy, K. S. Murray and B. O. West, *Inorg. Chem.*, 1985, **24**, 1561–1567.
- T. E. Westre, P. Kennepohl, J. G. DeWitt, B. Hedman, K. O. Hodgson and E. I. Solomon, *J. Am. Chem. Soc.*, 1997, **119**, 6297–6314.
- A. Roe, D. Schneider, R. Mayer, J. Pyrz, J. Widom and L. Que Jr., *J. Am. Chem. Soc.*, 1984, **106**, 1676–1681.
- (a) J. Sanders-Loehr, W. D. Wheeler, A. K. Shiemke, B. A. Averill and T. M. Loehr, *J. Am. Chem. Soc.*, 1989, **111**, 8084–8093; (b) H. Zheng, Y. Zang, Y. Dong, V. G. Young, Jr. and L. Que, Jr., *J. Am. Chem. Soc.*, 1999, **121**, 2226–2235.
- J. Cho, J. Woo and W. Nam, *J. Am. Chem. Soc.*, 2010, **132**, 5958–5959.
- (a) S. Fukuzumi, *Coord. Chem. Rev.*, 2013, **257**, 1564–1575; (b) W. Nam, Y.-M. Lee and S. Fukuzumi, *Acc. Chem. Res.*, 2014, **47**, 1146–1154.
- J. Yano and V. Yachandra, *Chem. Rev.*, 2014, **114**, 4175–4205.
- P. E. Siegbahn, *Acc. Chem. Res.*, 2009, **42**, 1871–1880.
- E. Y. Tsui, J. S. Kanady and T. Agapie, *Inorg. Chem.*, 2013, **52**, 13833–13848.
- Z. Codolà, L. Gómez, S. T. Kleespies, L. Que Jr., M. Costas and J. Lloret-Fillol, *Nat. Commun.*, 2015, **6**, 5865, DOI: 10.1038/comms6865.

